IMAGE-RAY TOMOGRAPHY

S. Dell and D. Gajewski

email: *sergius.dell@zmaw.de*
keywords: *Image-ray tomography*

ABSTRACT

Tomographic methods for the determination of velocity models using kinematic wavefield attributes strongly depend on the accuracy of the attributes. The Common-Reflection-Surface method applied to prestack data provides the attributes already with high quality. However, one difficulty of the CRS method is the treatment of diffractions and triplications, especially when located close to reflections. In such areas the quality of the attributes is not sufficient and, therefore, velocity model building with Normal Incident Point wave tomography does not provide an optimum result. In this context, it is reasonable to extract the kinematic wavefield attributes in the time-migrated domain. The Common-Reflection-Surface method applied to the time-migrated data approximates the zero-offset traveltime as a second-order Taylor expansion in the vicinity of the image ray. The data vector for the inversion containts traveltimes and wavefront curvatures of the image rays. The model vector is calculated by dynamic ray-tracing along central image rays. The inversion problem is solved iteratively by computing the least-squares solution to the locally linearized problem during each iteration step. The required Fréchet derivatives for the tomographic matrix are calculated with ray perturbation theory.

INTRODUCTION

The construction of velocity models is an important task for seismic depth imaging. The Normal-Incident-Point (NIP) wave tomography established as a powerful method for initial depth model building. The NIP wave tomography makes use of kinematic wavefield attributes like wavefront curvatures and emergence angles extracted from prestack data with the CRS stack (Duveneck, 2004). The inversion is based on the criterion that for a consistent velocity model all considered NIP waves focus at zero traveltime when propagated back into the subsurface along the normal rays. However, the reliable determination of kinematic wavefield attributes of reflections close to triplications and diffractions is complicated. The potential errors in attributes affect the inversion process or may even lead to an erroneous velocity model. Therefore, we propose to make use of kinematic wavefield attributes extracted in the time-migrated domain, where diffractions have been collapsed and triplications unfolded.

The key point of the proposed inversion algorithm is the image-ray consept. The image-ray concept was proposed by Hubral (1977) to give the theoretical explanation of time migration. During the time migration the energy distributed in the vicinity of the stationary point is focused around the apex position of the time-migration operator. The image ray connects a depth point with the apex position of the time-migration operator. The image ray is normal to the measurements surface and travels down to hit the reflector at the Image-Incident-Point (IIP), where the incidence angle usually is not normal to the reflector. Considering a point source exploding at the IIP. The wave which starts to propagate to the surface is called Image-Incident-Point wave. The corresponding ray is the image ray. So far, the concept of the image rays is limited to poststack imaging and the computation of the image rays is done through ray tracing. Unfortunately, the ray tracing is very sensitive to the initial time-migration velocity model. Therefore, an update of the time-migration velocity model is usually performed to smooth and improve it before the ray tracing. Moreover, the time-migrated velocities are frequently transformed in time-interval velocities by

Dix inversion (Cameron et al., 2007; Iversen and Tygel, 2008). This transformation contributes to potential errors in the velocity model making the image ray tracing insufficient and inefficient.

The CRS stack applied to the time-migrated data approximates the zero-offset reflection traveltime as a second-order Taylor expansion in image point coordinates, in the vicinity of the central image ray. However, the direct extraction of the wavefront curvature of the image ray in prestack time-migrated date is complicated because they should vanish if the seismic data are perfectly time-migrated. Thus we propose to apply a CRS like multiparameter stack to Common-Scatter-Point data. To avoid the ambiguity in the notation, we reffer this multiparameter stack as Common-Scatter-Point-Surface (CSPS) stack. The CSP data are time-migrated gathers with a hyperbolic moveout which is based on the surface distance from a scatterpoint location to a collocated source and receiver. The CSP gathers are generated from the CMP gathers by the CSP data mapping (Dell et al., 2009). The CSP data mapping is based on the parametrization of the double square root (DSR) operator for the common offset (CO) operator apex. The parametrized time migration operator assigns stacked amplitudes directly into its CO apex while the conventionally migration operator assigns the stacked amplitudes into its ZO apex. The CSPS stack applied to the CSP data provides reflector dip and curvature of time-migrated reflections as well as the wavefront curvature of the image ray, the wavefront curvature of the IIP-wave. Note that the model-based dip and curvature of reflector can be interpreted in terms of real reflector dip and curvature in depth (Tygel et al., 2009).

Similarly to the NIP-wave, we can use the curvature of the IIP-wave to construct the depth velocity model. The velocity model is consistent with the data, if all considered IIP-waves focus at zero traveltimes when propagated back into the subsurface. The data vector for the inversion containt traveltimes and wavefront curvatures of the IIP-waves extracted from CSP data. The model vector is calculated by dynamic ray-tracing along image rays. The inversion problem is nonlinear because results of the dynamic ray tracing depend on the model parameters. Instead of solving a global nonlinear optimization problem, the inversion problem is solved iteratively by computing the least-squares solution to the locally linearized problem during each iteration step. The required Fréchet derivatives for the tomographic matrix are calculated with ray perturbation theory. Application to 2D synthetic data demonstrates the potential of the method to obtain a smooth velocity model

In the next section, we explain the theoretical background of the proposed method for the tomographic inversion. We start with a review of the image-ray concepts, then we briefly discuss the CSPS stack of time-migrated reflections, and finish with the formulation of the inversion problem.

THEORY

Review of the image ray concept

Before describing the tomography based on the IIP-waves, we first review Hubral's image-ray concept for time migration. Time migration is based on the duality that the diffraction and reflection traveltime surface of a depth point in the subsurface are tangent at the stationary point in the time-domain (Fig. 1). During time migration the energy distributed in the vicinity of the stationary point is focused around the apex position of the time-migration operator. To determine the depth position of the focused energy, Hubral introduced the concept of the image ray (Hubral, 1977). The image ray connects a depth point with the surface position of its image, i.e., it is the propagation path of the energy to the apex position of the time-migration operator. Because diffraction surfaces have zero time-slope at their apex positions, all image rays hit normal at the acquisition surface.

These rays are naturally vertical only in a medium with constant velocity. In an inhomogeneous medium with more complex velocity distribution, they behave in a similar way as normal incident rays: below a curved interface their refraction obeys Snell's law. The image rays relate to time-migrated reflections in a similar way as normal incidence rays relate to primary reflections. Time-migrated primary reflections can be obtained by tracing image rays vertically down from the surface to the desired reflector at depth.

The propagation of the image rays can be described by kinematic ray tracing. In a 3-D medium with a smooth velocity distribution, the kinematic ray tracing can be formulated by the ordinary differential equations (see, e.g., Červený (2001); Popov (2002)).

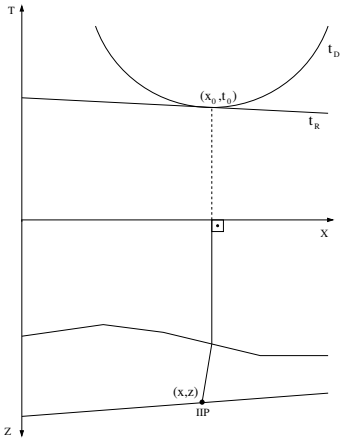

Figure 1: 2-D subsurface iso-velocity layer model. Suppose an image ray connects surface point x_0 and subsurface point (x, z), and the two-way traveltime along this ray is t_0. The energy diffracted from a point scatterer at IIP with coordinates (x, z) is distributed along the diffraction surface whose apex is at (t_0, x_0).

$$\begin{aligned} \frac{\partial \mathbf{x}}{\partial \tau} &= v^2 \mathbf{p}\,, \\ \frac{\partial \mathbf{p}}{\partial \tau} &= v \nabla \frac{1}{v}\,, \end{aligned} \tag{1}$$

with the initial conditions $\mathbf{x} = (x_1, x_2, x_3) = \mathbf{x}_0$ and $\mathbf{p} = 0$. The time τ is the parameter along the rays. Furthermore, we consider the natural orthogonal basis. As has been shown (see, e.g., Červený (2001); Popov (2002)), the dynamic ray-tracing represents a system of ordinary differential equations

$$\begin{aligned} \frac{\partial \mathbf{Q}}{\partial \tau} &= v^2 \mathbf{P}\,, \\ \frac{\partial \mathbf{P}}{\partial \tau} &= \mathbf{V}\mathbf{Q}\,, \end{aligned} \tag{2}$$

where $\mathbf{V}$ is a symmetric matrix

$$\mathbf{V} = -\frac{1}{v}\frac{\partial^2 v}{\partial x_i \partial x_j}(\vec{e}_2)_i(\vec{e}_3)_j\,, \tag{3}$$

and $\mathbf{Q} = \frac{\partial \mathbf{x}}{\partial x_i}$, and $\mathbf{P} = \frac{\partial \mathbf{p}}{\partial x_i}$.

A matrix $\mathbf{M}\left(M_{ij} = \partial^2 t/\partial x_i \partial x_j,\ i, j = 1, 2\right)$ of second derivatives of traveltime can be determined as

$$\mathbf{M} = \mathbf{P}_2 \mathbf{Q}_2^{-1}\,. \tag{4}$$

This allows to approximate second-order traveltimes of a specified wave at arbitrary points near a reference ray by dynamic ray-tracing along that ray. If a point on the reference image ray is specified by $\mathbf{x} = x_i,\ i = 1, 2$, the second-order traveltime approximation at point $\mathbf{x} + \Delta\mathbf{x}$ is available and given by

$$t(\mathbf{x} + \Delta\mathbf{x}) = t(\mathbf{x}) + \mathbf{p}\Delta\mathbf{x} + \frac{1}{2}\Delta\mathbf{x}^t \mathbf{M} \Delta\mathbf{x}\,. \tag{5}$$

If we square this expression, retain only the terms up to second order in $\mathbf{x}$, and take into account the initial conditions for image rays, we obtain finally the traveltime approximation for paraxial image rays in the

vicinity of the central image ray, i.e.,

$$t^2 = t(\mathbf{x})^2 + t(\mathbf{x})\ \Delta\mathbf{x}^t\mathbf{M}\Delta\mathbf{x}\,. \tag{6}$$

In the next section, we briefly review some aspects of the application of the CSPS stack to time-migrated reflections. We also establish a relation between the wavefront curvature of the image ray and the kinematic wavefield attributes of time-migrated reflections.

Common-Scatter-Point-Surface stack of time-migrated reflections

To obtain time-migrated reflections, we transform Common Midpoint (CMP) gathers into Common Scatter Point (CSP) gathers with the help of the CSP data mapping (Dell et al., 2009). The CSP data mapping is based on the parametrization of the DSR equation with the CO apex time. This parametrization allows to assign the migration output directly into the CO apex of the time-migration operator as described in appendix A. A CSP gather collects all scattered energy along a 3D diffraction traveltime surface defined by t(m,h) (see Fig. 2a) and distributes this energy along a 2D hyperbolic path defined by t(h) (see Fig. 2b). When a scatter point is exactly at the output location of a CSP gather, its scattered energy is constructively stacked along this hyperbolic path, i.e., diffractions collapse during this process. Energy from scatter points displaced from the output location is canceled through destructive interference. More details about CSP gathers can be found in Bancroft et al. (1998). The CSP building process is depicted schematically in Figure 2.

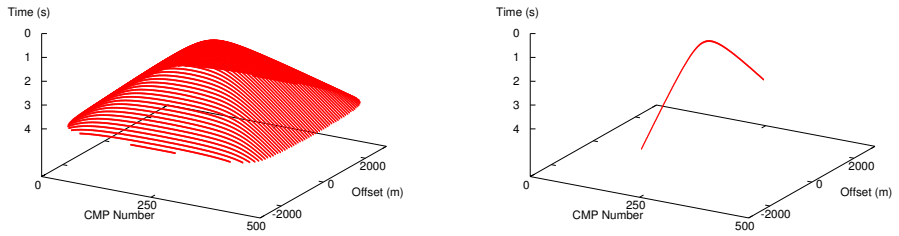

(a) **(b)**

Figure 2: The traveltime surface $t(m,h)$ for a single scatter point (a). The traveltime surface is known as the Cheops pyramid. The CSP gather formed by collapsing the Cheops pyramid to a hyperbola in the $m=0$ plane. The apex of the hyperbola lays at (m_0, t_0).

The moveout in the CSP gather is based on the distances from a collocated source and receiver to a scatter point location and not on the source-receiver offset as for a CMP gather. There is no directional dependency in the traveltime and, therefore, no reflection point smearing for inclined reflectors. Due to the increased reflector resolution and the absence of diffractions stacking parametersÂămay be estimatedÂă more accurately in the CSP gathers then in the CMP gathers.

In the time-migrated domain, the Common-Scatter-Point surface is given in terms of image point coordinates (ξ, ζ, T^M), where ξ specifies the scatter-point displacement with respect to the considered CSP, ζ is the scatter-point offset which is a half of the distance from the scatter-point location to the collocated source and receiver. For the sake of simplicity, we will use notation *offset* instead of *scatter-point offset*.

Now we consider the Taylor zero offset (ZO) hyperbolic approximation of the time-migrated reflection traveltime with respect to scatter-point displacement and half-offset

$$T^M(\xi,\zeta)^2 = \left(T_0^M + \Delta\xi^t p^M\right)^2 + T_0^M\left(\Delta\xi^t M^M_{\xi\xi}\Delta\xi + \Delta\zeta^t M^M_{\zeta\zeta}\Delta\zeta\right)\,, \tag{7}$$

where

$$T_0^M = T^M(\xi_0, \zeta = 0)$$

$$p^M = \left(\frac{\partial T^M}{\partial \xi_i} \right)$$

$$M^M_{\xi\xi} = \left(\frac{\partial^2 T^M}{\partial \xi_i \partial \xi_j} \right)$$

$$M^M_{\zeta\zeta} = \left(\frac{\partial^2 T^M}{\partial \zeta_i \partial \zeta_j} \right) \tag{8}$$

The expression above is formally identical to the CRS operator. It describes the traveltimes of paraxial image rays that are incident on the same reflector as the central image ray. Their incident points are situated in the vicinity of the incident point of the central image ray. Therefore similar to the CRS method, where we consider a continuous surface around the NIP, we consider a continuous surface around the IIP. The time T_0^M is twice the traveltime along the central image ray from the reference point on the measurements surface to the IIP. The matrix $M^M_{\xi\xi}$ is related to the curvature of the reflector and p^M to the reflector dip (Tygel et al., 2009). Note that both parameters are model-based whereas CRS attributes are related to wavefield parameter in the acquisition surface. Below we will show that the matrix $M^M_{\zeta\zeta}$ is related to the wavefront curvature of the image ray.

In order to find a physical interpretation of $M^M_{\zeta\zeta}$, the expression for the CSPS operator for a time-migrated reflection given by Eq. 7 is restricted to a single CSP., i.e., $\Delta\xi = 0$:

$$t(\zeta)^2 = t_0^2 + t_0 \, \Delta\zeta^t M^M_{\zeta\zeta} \Delta\zeta \tag{9}$$

Comparing this equation with the traveltime approximation for paraxial rays in Equation 6, we see that the matrix $M^M_{\zeta\zeta}$ is linked to the wavefront curvature of the image ray.

Similar to the NIP-wave experiment (Chernyak and Gritsenko, 1979; Hubral and Krey, 1980), we can consider an IIP-wave experiment. The experiment can be carried out by placing a point source in the IIP of the central image ray. The IIP-wave propagates along a central image ray to the measurement surface (Fig. 3). Note that for an image ray the slowness projection on the tangent plane to the emergence location at its initial point vanishes. Therefore, at the emergence location $(\xi = 0, \zeta)$ the central image ray is determined only in terms of the curvature of the IIP wave K_{IIP}.

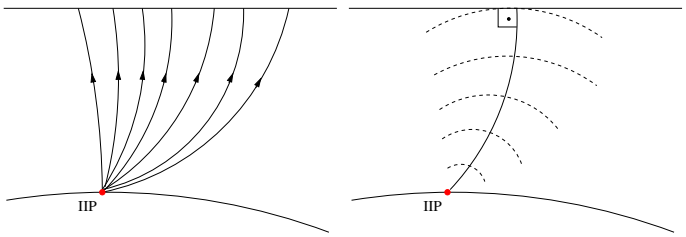

Figure 3: The ray trajectories associated with a hypothetical wave caused a point source at the IIP (IIP wave). Geometrically, the CSP ray segments build the IIP wave (a). In a consistent velocity model, IIP waves focus at the IIP at zero traveltime, when they are propagated back in the time-migrated domain (b).

In the 2-D case, the matrix M^M_ζ of second derivatives of the migrated traveltime is given by

$$M^M_\zeta = \frac{\partial^2 T^M}{\partial^2 \zeta} = A K_{IIP}$$

where A is a constant including the near-surface velocity and K_{IIP} is the wavefront curvature of the image ray.

In the next section, the the wavefront curvature of the image ray will be used to formulate a tomographic inversion method for the determination of smooth isotropic velocity models. The method is introduced for the 2-D case. The extension to 3-D velocity models, however, is straight forward.

Methodology of Image-Ray Tomography

The parameters describing the second-order traveltimes of emerging IIP wavefronts in the vertical plane defined by the seismic line are the image ray traveltime T_0^M and the second spatial traveltime derivatives $M(\zeta)$ at the image ray emergence location ξ_0. The data required for the 2D tomographic inversion, thus, consist of data points

$$(T^M, M^M, \xi)_i,\ i = 1, ..., n_{data}\,. \tag{10}$$

The data are extracted from the results of the 2D CSPS stack at n_{data} pick locations. Each of these data points is associated with a IIP in the subsurface, characterized by its spatial location $(x, z)^{(IIP)}$. The 2-D velocity model is described by two-dimensional B-splines

$$v(x, z) = \sum_{j=1}^{n_x} \sum_{k=1}^{n_z} v_{jk} \beta_j(x) \beta_k(z) \tag{11}$$

where m_{jk} are B-spline coefficients representing the velocity model on a rectangular grid, n_x and n_z are the numbers of grid points in the horizontal and vertical directions. For the 2-D tomographic inversion, the model is therefore defined by the model parameters:

$$\begin{aligned} &(x, z)_i^{(IIP)},\ \ i = 1, ..., n_{data} \\ v_{jk}\ \ &j = 1, ..., n_x; k = 1, ..., n_z\,. \end{aligned} \tag{12}$$

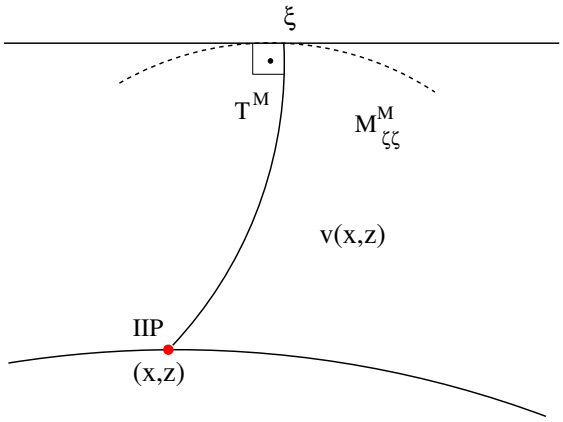

Figure 4: Definition of data and model components for 2D tomographic inversion. The data components describe the second-order traveltime curve associated with an emerging IIP wavefront and consist of triples $(T^M, M^M_{\zeta\zeta}, \xi)$. The corresponding IIP model components are the spatial location of the IIP with coordinates (x,z), while the velocity field $v(x, z)$ is determined as the B-spline coefficients.

The forward modeling of the quantities $(T^M, M^M_{IIP}, \xi)_i^{mod},\ i = 1, ..., n_{data}$ during the inversion process is performed by applying 2-D kinematic and dynamic ray tracing. Kinematic ray tracing yields the emergence location ξ_0 of the image ray, while integration of equation 1 along the image ray yields the traveltime T_0^M.

It has been shown above that the parameters describing a second-order approximation of the traveltimes of emerging IIP wavefronts can be extracted from the CSP data by applying the CSPS stack. The kinematic wavefield attributes of time-migrated reflections describe the emerging hypothetical IIP wavefront in terms of second traveltime derivatives. In 2-D orthonormal coordinates, the second spatial derivative of the IIP-wave traveltime on the central image ray is given as

$$M_{IIP} = P_2 Q_2^{-1}\,.$$

For the numerical solution of the kinematic ray-tracing system and the dynamic ray-tracing system with fourth-order Runge-Kutta scheme is used. For the tomographic matrix, the Fréchet derivatives of the modeled data components with respect to the model parameters are needed. These are calculated during ray tracing by applying ray perturbation theory (e.g., (Červený, 2001; Farra and Madariaga, 1987))

$$\frac{\partial\left(T^M, M_\xi^M, \xi\right)}{\partial\left(x, z, v\right)}.$$

The inverse problem to be solved can be formally stated as follows: a model vector **m**, consisting of the velocity model parameters $v_{jk},\ j = 1, ..., n_x,\ k = 1, ..., n_z$ and image ray starting parameters at depth $(x, z)_i,\ i = 1, ..., n_{data}$, is sought, that minimizes the misfit between the data vector **d**, containing the picked values, and the corresponding modeled values $\mathbf{d}_{mod} = \mathbf{f}(\mathbf{m})$. The operator **f** symbolizes the dynamic ray tracing in the given model. As a measure of misfit the least-square norm is used (Tarantola, 1987). The modeling operator **f** is non linear, hence a solution to the inverse problem is found in an iterative way by locally linearising **f** and applying linear least-squares minimization during each iteration.

In the next section, we demonstrate the potential of the new method to build a smooth migration velocity model using curvatures of the wavefront of the image rays. We present applications using synthetic data for a simple model.

SYNTHETIC EXAMPLE

As a first test, the image-ray based tomographic algorithm was applied to a synthetic example. Figure 8a displays a simple synthetic model with an anticline in the middle. The model consists of 3 layers. The velocity in the first layer is 1500 m/s, in the second layer 2300 m/s, in the third layer 2700 m/s. The synthetic seismograms were generated by a ray tracer package kindly provided by NORSAR Innovation AS. We used a Ricker-wavelet with prevailing frequency of 25 Hz. The sampling interval is 2 ms and the used recording time is 2.4 s. Finally, Gaussian noise was added to the prestack data. The signal-to-noise ratio is 20. CMP gathers are displayed in Figure 9. The CRS stacked section displays triplications caused by the anticline structure (Fig. 5a).

Firstly, the automatic CMP stack was applied to prestack gathers to determine stacking velocities. The stacking velocities served then as migration velocities to generate CSP gathers. Afterwards, the CSPS stack was applied to CSP gathers to extract curvatures of the IIP-waves. Figure 5 shows the CRS and CSPS stack section. Triplications, which are present in the CRS stack section, are unfolded in the CSPS stack section (Fig. 5b).. The considerable high focusing of the triplications indicates that time-migration velocities were correctly determined. Also, the CSPS stack provides a higher coherency section (Fig. 6). Especially for the top of the anticline, we observe a significant rise of the coherency value in comparison to the coherency section provided by the CRS stack. The coherency value is crucial for the automatic picking of data vectors components in the proposed inversion process. The high coherency value confirms the reliability of the kinematic wavefield attributes and allows to prove if the pick location under consideration is actually part of a reflection event by checking of coherency values for neighboring samples. Also, the low coherency value lead to a decrease of the searched-for coherency maxima and, therefore, an increase of picks number that causes arisen computation costs.

Figure 7 illustrates the sections of the NIP-wave radii (a) and IIP-wave-radii (b). In the NIP-wave radii section, we observe an unphysical behavior when triplications are closed to the reflection. In that area, the NIP-wave radii become discontinuous. In the contrast, the IIP-wave radii do not have any discontinuities.

After the application of the CSPS stack, 592 data points (T^M, M^M, ξ) were picked in the resulting simulated ZO time-migrated section and associated CSPS attribute sections. These served as input for the inversion. The velocity model consists of 104 B-spline knots: 8 knots in the x-direction with a spacing of 1000m and 13 knots in the z-direction with a spacing of 200m. The starting model was chosen to consist of a near-surface velocity of 1500 m/s and a vertical velocity gradient of 0.6 s^{-1}. To find the initial ray starting positions of the image ray in the subsurface, rays corresponding to locations of all data points were simply traced downward in the initial model normal to the acquisition line until the one-way traveltime T^M was reached.

The inversion result after 11 iteration is shown in the Figure 8b. The calculated image rays are also depicted. One can observe that the image rays are normal to the surface. Note that the model obtained as a

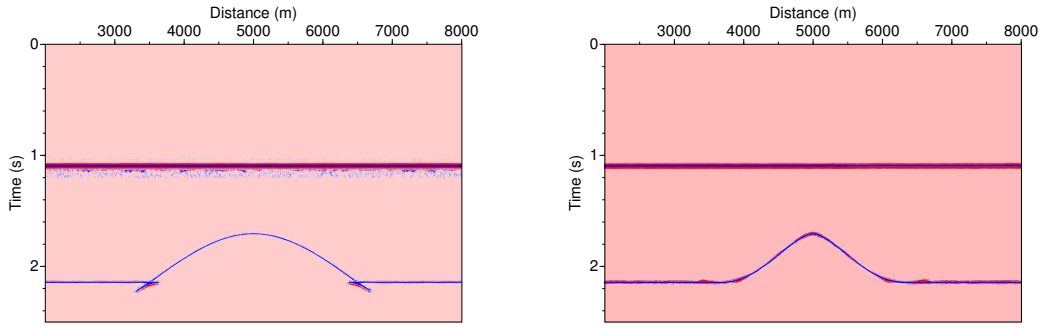

(a) **(b)**

Figure 5: Stacks of the simple synthetic model with an anticline (Fig. 8a). The CRS stacked section (a) displays triplications caused by the anticline structure and no triplications. The CSPS stacked section (b) shows the anticline structure. Amplitudes of both sections were weighted with the corresponding coherency.

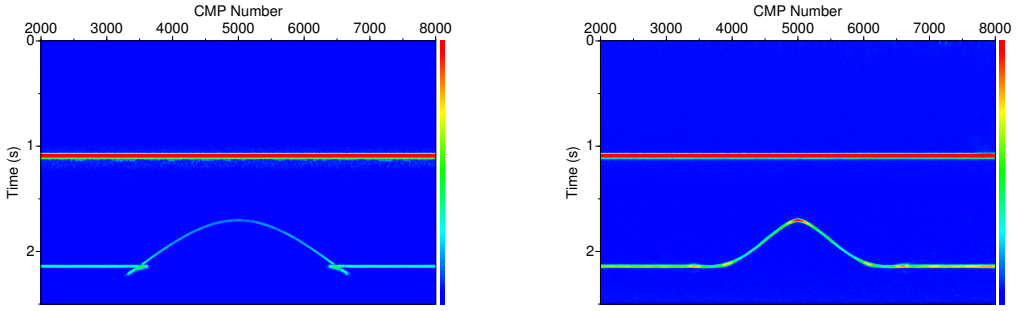

(a) **(b)**

Figure 6: Coherency sections obtained by the CRS stack (left) and the CSPS stack (right). In the latter one, we observe higher coherency values for the second reflection. The high coherency value is crucial for picking of events in tomography methods.

result of the tomographic inversion is described by smooth spline functions, while the true model is blocky. The resolution of the obtained model depends on the grid spacing. However, the inversion result should be kinematically equivalent to the true model for all reflection events in the data. Figure 8b shows that the reconstructed model resembles a smoothed version of the true velocity distribution. The resulting smooth velocity model was finally used to perform prestack depth migration to investigate whether reflectors in the model are correctly imaged.

For that purpose, a Kirchhoff migration algorithm based on eikonal traveltimes was used.

Figure 10 shows a stack of all common-offset migrations between 0 and 2000 m offset. Before the stacking, the Common Image Gathers (CIG) were muted according Figure 9. As expected from the results of Figure 11, all reflectors in the migrated image are correctly positioned. The bow-tie events in the seismic data due to the anticline structure have been correctly unfolded.

Figure 11 shows some CIGs at regularly spaced image locations with a separation of 1000 m. Each CIG represents the migration result at the respective image location as a function of offset. The offsets displayed in the CIGs in Figure 11 range from 0 to 2000 m. At shallow depths and large offsets, a mute has been applied to remove events with excessive wavelet stretch.

The velocity model is consistent with the seismic data if the results of prestack depth migration are

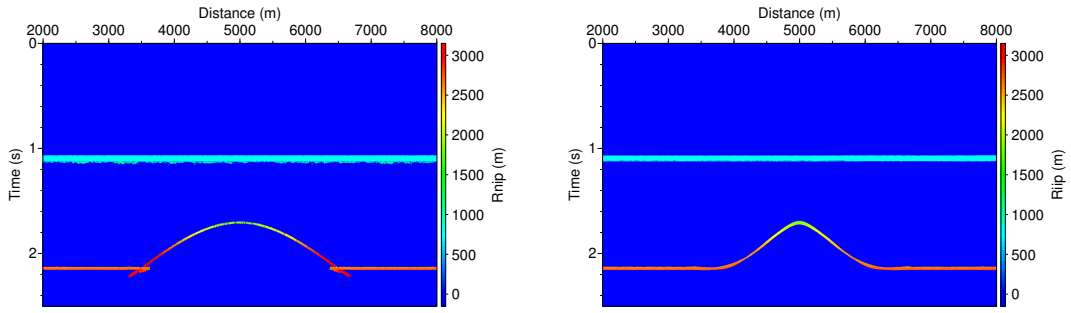

(a) **(b)**

Figure 7: R_{NIP} section (left) and R_{IIP} section (right). In the R_{NIP} section, we observe the ambiguity of the wavefield attribute determination closed to triplications. Contrastingly in the R_{IIP} section, the determination of the wavefield attribute is easy. Note that the both sections were weighted with the corresponding coherency.

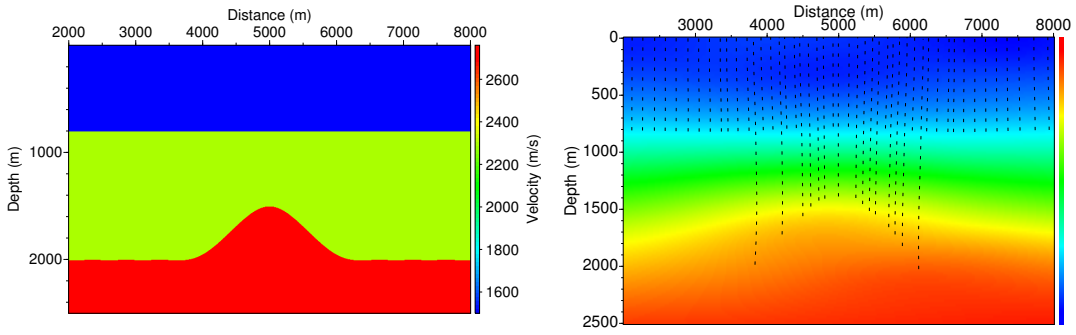

(a) **(b)**

Figure 8: A simple synthetic model with an anticline in the middle and inversion result of the IIP wave tomography. The model consists 3 layers. The velocity in the first layer is 1500 m/s, in the second layer 2300 m/s, in the third layer 2700 m/s. The reconstructed velocity model is displayed with image rays. The input data for the inversion were picked from the CSPS Stack applied to the CSP data and associated CSPS attribute sections.

kinematically independent of offset. The events in the CIGs displayed in Figure 11 are almost flat. This confirms that the model obtained with the proposed tomographic inversion is kinematically correct and suitable for further velocity model building techniques like migration velocity analysis.

The synthetic data example presented in this section shows that the concept of using the wavefront curvatures of the image rays for the construction of smooth, laterally inhomogeneous velocity model leads to a velocity model that is consistent with the data. The applicability of the presented method is limited since input data for the inversion are model-based. The inversion depends on the accuracy of the time-migration velocities used for the generation of CSP data. In case of strong lateral velocity variations, it is limited by the size of the offset aperture and by the strength of the velocity variation. Good result are achieved only if the hyperbolic assumption is applicable, i.e., for moderate lateral velocity variation in the seismic data.

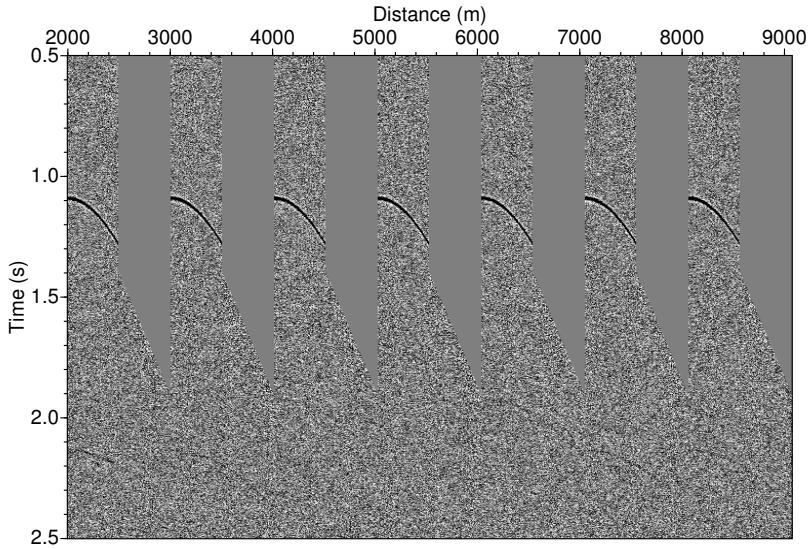

Figure 9: CMP gathers. Note that because of higher noise level in the data the second reflection is not observerable in the CMP gathers.

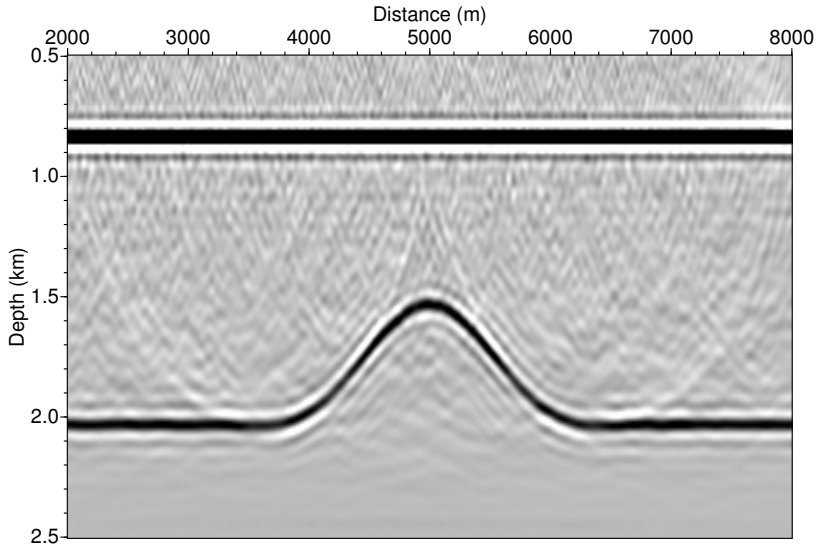

(a)

Figure 10: A simple synthetic model with an anticline in the middle. The depth-migrated section of CMP data using the tomographic model of 8b.

CONCLUSIONS

We have presented a new tomographic method for building smooth velocity models for depth imaging based on wavefront curvatures of the image rays. These wavefront curvatures can be extracted from Common

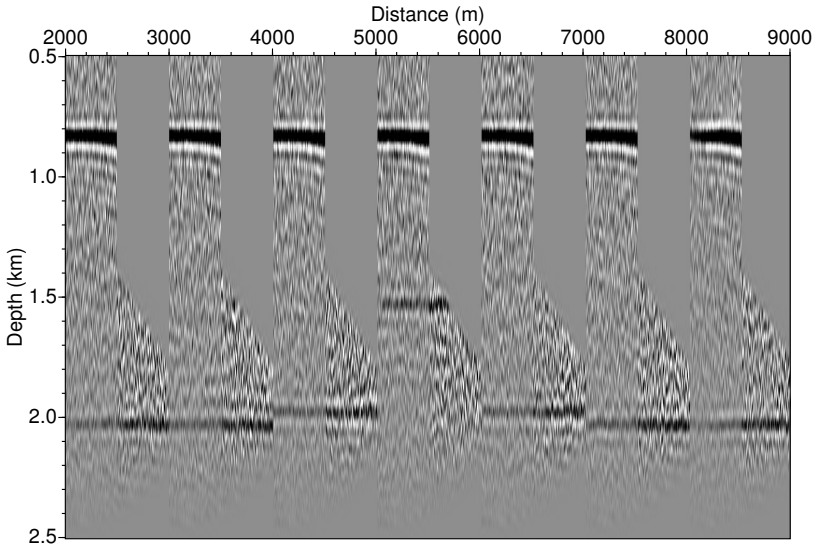

Figure 11: CIGs after prestack depth migration.The offsets displayed in the CIGs range from 0 to 2000 m. At shallow depths and large offsets, a mute has been applied to remove events with excessive wavelet stretch. The events in the CIGs are almost flat.

Scatter Point gathers by Common-Scatter-Point-Surface stacking. The Common Scatter Point gathers are prestack time-migrated data with a hyperbolic moveout which is based on the surface distance from a scatterpoint location to a collocated source and receiver. One of the advantages of CSP data is the absence of diffractions and triplications. Therefore, the estimated attributes are less affected by conflicting NIPs and ambiguity compared to CRS stack and NIP-wave tomography.

The method can be seen as an additional tool to provide constraints for kinematic velocity model building. It is particularly useful in the areas where diffractions and triplications are located close to reflections.

The method has been successfully tested on a synthetic data example.

ACKNOWLEDGMENTS

The authors would like to thank the sponsors of WIT consortium for the support. We thank NORSAR Innovation AS for kindly permition to use NORSAR ray tracing package. We also thank TGS for kindly providing the data. We are grateful to Boris Kashtan and Martin Tygel for helpful discussions.

REFERENCES

Bancroft, J., Geiger, H., and Margrave, G. F. (1998). The equivalent offset method of prestack time migration. *Geophysics*, 63:2042–2053.

Baykulov, M. and Gajewski, D. (2009). Prestack seismic data enhancement with partial common-reflection-surface (CRS) stack. *Geophysics*, 74:no. 3, V49–V58.

Cameron, M. K., Fomel, S. B., and Sehian, J. A. (2007). Seismic velocity estimation from time migration. *Inverse Problems*, 23:1329–1369.

Chernyak, V. S. and Gritsenko, S. A. (1979). Interpretation of the effective common-depth-point parameters for a three-dimensional system of homogeneous layers with curvilinear boundaries. *Geologiya i Geofizika*, 20:112–120.

Dell, S., Gajewski, D., and Vanelle, C. (2009). Common Scatter Point data mapping. In *Annual Report No. 13*, pages 43–57. Wave Inversion Technology Consortium.

Duveneck, E. (2004). *Tomographic determination of seismic velocity models with kinematic wavefield attributes*. Logos Verlag Berlin.

Farra, V. and Madariaga, R. (1987). Seismic wavefront modeling in heterogeneous media by ray perturbation theory. *Geophys. Res.*, 92:2697–2712.

Hubral, P. (1977). Time migration – Some ray theoretical aspects. *Geophysical Prospecting*, 25:738–745.

Hubral, P. and Krey, T. (1980). *Interval velocities from seismic refflection traveltime measurements*. Soc. Expl. Geophys.

Iversen, E. and Tygel, M. (2008). Image-ray tracing for joint 3D seismic velocity estimation and time-to-depth conversion. *Geophysics*, 73, n.3:S99–S114.

Popov, M. M. (2002). *Ray Theory and Gaussian Beam Method for Geophysicists*. EDUFBA, Salvador Bahia.

Tarantola, A. (1987). *Inverse problem theory:Methods for data fitting and model parameter estimation*. Elsevier, Amsterdam.

Tygel, M., Ursin, B., Iversen, E., and de Hoop, M. V. (2009). An interpretation of CRS Attributes of time-migrated reflections. *WIT Reports*, Annual Report No. 13:260–268.

Červený, V. (2001). *Seismic ray theory*. Cambridge University Press, Cambridge.

APPENDIX A

Parametrization of the DSR equation

The Kirchhoff time migration operator is given by the double square root (DSR) equation.

$$t_D = \sqrt{\frac{t_0^2}{4} + \frac{(m-h)^2}{v^2(t_0)}} + \sqrt{\frac{t_0^2}{4} + \frac{(m+h)^2}{v^2(t_0)}}\,, \tag{13}$$

where t_0 is the image time that corresponds to the zero offset (ZO) operator apex, m is midpoint displacement, h is half source-receiver offset, and v is the migration velocity. The DSR operator can be parametrized with the CO apex time t_{apex}

$$t_{apex} = \sqrt{t_0^2 + \frac{4h^2}{v^2(t_0)}}\,. \tag{14}$$

$$\begin{aligned} t_D &= \sqrt{\frac{t_0^2}{4} + \frac{m^2 - 2mh + h^2}{v^2(t_0)}} + \sqrt{\frac{t_0^2}{4} + \frac{m^2 + 2mh + h^2}{v^2(t_0)}} \\ &= \sqrt{\frac{t_0^2}{4} + \frac{h^2}{v^2(t_0)} + \frac{m^2 - 2mh}{v^2(t_0)}} + \\ &+ \sqrt{\frac{t_0^2}{4} + \frac{h^2}{v^2(t_0)} + \frac{m^2 + 2mh}{v^2(t_0)}} \end{aligned} \tag{15}$$

Finally,

$$t_D = \sqrt{\frac{t_{apex}^2}{4} + \frac{m(m-2h)}{v^2(t_0)}} + \sqrt{\frac{t_{apex}^2}{4} + \frac{m(m+2h)}{v^2(t_0)}} \tag{16}$$

Now we parameterize every CO section with the CO apex of the migration operator t_{apex}. This means that we assume that every sample in a CO section coincides with a corresponding CO apex time. However, the velocity in the equation 16 still depends on the ZO apex of the migration operator t_0. For the determination of $v(t_0)$ for the considered apex time t_{apex} a similar iterative search procedure as described in Baykulov and Gajewski (2009) is used. Fig. 12 compares principles of the prestack time migration and the CSP data mapping.

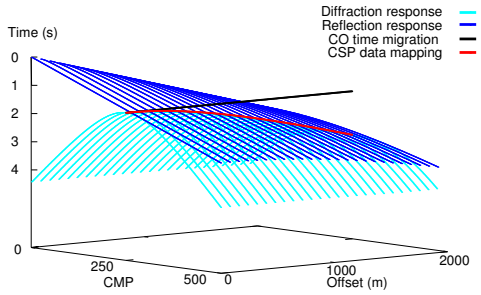

Figure 12: The reflection response for a homogeneous model with a dipping reflector is depicted in blue. The migration operator for one CMP is depicted in cyan. The migration output is usually assigned to the ZO operator apex for every CO section (black line). Contrastingly, the mapped output is assigned to the CO operator apex for every CO section (red line).